POLYPUBLIE
Polytechnique Montréal

POLYTECHNIQUE MONTRÉAL
UNIVERSITÉ D'INGÉNIERIE

Document en libre accès dans PolyPublie
Open Access document in PolyPublie

Document publié chez l'éditeur officiel
Document issued by the official publisher

Article

Production of Monodisperse Large Drop Emulsions by Means of High Internal Phase Pickering Emulsions—Processing and Formulation

Mina Saghaei, Edith Roland Fotsing, Annie Ross, and Louis Fradette*

Read Online

ACCESS | Metrics & More | Article Recommendations | SI Supporting Information

ABSTRACT: High internal phase Pickering emulsions (HIPPE) have received significant research attention in the last two decades due to their potential for a wide range of applications. The appropriate processing of such high-viscosity emulsions, hundreds of times more viscous than that of the continuous phase, and the control of the final droplet size remain challenges to be tackled. Our research targeted this knowledge gap by examining the influence of the emulsion formulation and the processing conditions on the final droplet size. The dispersed phase fraction (100 cSt silicon oil) ranged between 75 and 80%. The emulsions were produced in a regular mixing tank equipped with a helical ribbon impeller rotating at a low speed (100−150 rpm). The effective viscosity of the continuous phase was obtained from the experimental torque measurements. The droplet size distributions were measured after emulsification and dilution in the continuous phases. It is shown that the capillary number obtained from the observed emulsification performance can help predict the final droplet size. Our approach provides a straightforward methodology to generate concentrated Pickering emulsions with controlled and predictable droplet size.
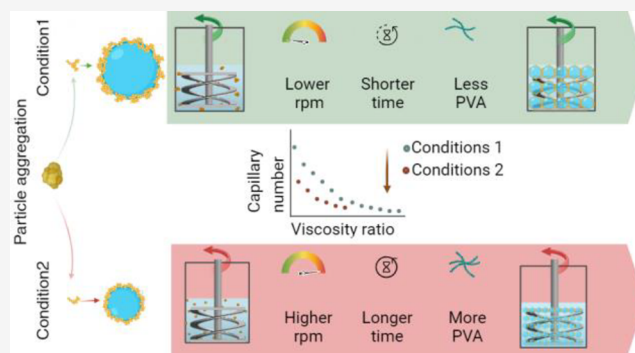
1. INTRODUCTION

Emulsions solely stabilized by solid particles at the oil−water interface were described by Ramsden and Pickering[1] about a century ago. Their behavior and properties have been actively investigated in recent decades,[3,4,6] along with some applications.[2−7] The substitution of solid particles for traditional surfactants in such emulsions (also known as Pickering emulsions) offers numerous advantages, making them ideal for applications in fields including biomedicine,[8,9] food,[10] fine chemical synthesis,[11] cosmetics,[12] and fine three-dimensional (3D) structures.[13−15]

The use of particles in the replacement of chemical surfactants not only strengthens the emulsion against coalescence but also lowers the risks of harmful surfactant release to the environment. Furthermore, the solid particles can be selected to suit some specific applications of the produced emulsions.[11,16,8,17−19]

Low-volume and energy-intensive apparatuses such as high-pressure homogenizers and ultrasonic probes are reported as emulsion generators.[20] However, high-pressure equipment produces small droplets with a considerable degree of polydispersity in the emulsion droplets.[21] Additionally, it may destroy the larger solid particles.[22] Other equipment to produce Pickering emulsions, including microchannels,[23] static mixers,[24,25] and membranes,[26] are limited for applications on larger scales, as the design of such equipment poses significant challenges.[20]

Large-capacity emulsification often requires the use of a high-speed rotating impeller in a mixing tank. Pitched blade turbines (PBT) have the capacity to emulsify large volumes of fluids and are known to generate larger droplets (>75 μm) compared to high-pressure homogenizers.[5,27] They are, however, limited to low-viscosity emulsification.

High internal phase Pickering emulsions (HIPPE) occur when the emulsion drops reach their maximum packing state. For spheres of size, the maximum packing value is around 74% (hexagonal close packing). When the emulsion reaches this packing state, the viscosity increases sharply and remains high thereafter. Similarly to dilute emulsions, a wide variety of particle types and particle sizes, oil types, and processing conditions are employed in the preparation of HIPPEs, and can be found in reviews.[19]

For high viscosities such as the ones encountered in concentrated emulsions, low-speed close-clearance impellers are more appropriate, as they natively deal with high-viscosity mixtures. Examples of such mixers are the Maxblend impeller,[28] anchor impellers,[29] Paravisc,[30] and helical ribbons (single-helical ribbon (SHR) and double-helical ribbon (DHR)).[30] Very few studies exist about the use of low-speed impellers applied to the production of emulsions. For instance, asphalt was successfully emulsified using an anchor impellor at 95% dispersed phase in surfactant-based emulsions.[29] Very narrow droplet size distributions and easy processing were demonstrated.

Viscous stresses generate the droplet breakup in the laminar flow,[31,32] while interfacial forces around the droplet will limit the extent of the breakup. The capillary number (Ca) represents the ratio of viscous forces to interfacial forces (Laplace pressure) from the shearing flow

$$Ca = \frac{\mu_c \dot{\gamma}}{2\sigma/D_{43}} \tag{1}$$

where μ_c represents the viscosity of the continuous phase, $\dot{\gamma}$ denotes the shear rate, σ is the interfacial tension between dispersed and continuous phases, and D_{43} is the diameter of a droplet. The droplet breaks if Ca exceeds a critical value (Ca_{crit}); the new droplets have smaller diameters and Ca becomes lower. Simultaneously, small droplets tend to coalesce, leading to increased diameter and Ca. Thus, the observed or effective capillary number of a given process will tend to "move toward" the critical capillary number if enough time is allowed for droplet rupture to occur repetitively.

Multiple empirical models predict the critical capillary number based on the viscosity ratio between the dispersed and continuous phases[33,31] and report the effect of viscosity ratio on the curvature of droplet breakage.[34] In these models, the Ca value is obtained for the dilute emulsion, where the effect of the neighboring droplets is neglected. This literature made use of constant viscosity for the continuous phase over the emulsification time. This assumption of constant continuous phase viscosity might not be accurate for Pickering emulsions where the continuous phase may be non-Newtonian and the presence of micron-sized particles induces more complexity.

HIPPEs not only exhibit a viscoelastic behavior themselves[35] but also the continuous phase might reveal complex rheological behavior. Depending on the particle size, shear rate, and repulsive force between particles, the continuous phase can exhibit both shear thinning and shear thickening,[36] as well as time-dependent behavior, thixotropy, and rheopexy.[37,38] The observed behavior is a complex function of the experimental conditions and formulation. The nonlinear rheological behavior of the concentrated suspension forming the continuous phase must be considered for calculating the viscosity ratio.

Despite extensive research on the fundamentals and properties of concentrated Pickering emulsions, there is still a lack of understanding regarding the control of the final droplet size and the impact of the processing conditions on HIPPEs in the laminar regime. This research aims to fill this gap by studying the impact of the process and formulation on the produced droplet size. This work seeks to develop methods for the precise control and estimation of droplet sizes under low shear rates.

2. MATERIALS AND METHODOLOGY

2.1. Materials. The dispersed phase for all emulsions was silicone oil with a viscosity of 100 cSt (Clearco Products Co., Inc.). The continuous phase was formed of an aqueous phase that contained dissolved poly(vinyl alcohol) (PVA) (Alfa Aesar) in distilled water at concentrations ranging from 2 to 4 wt %. Polyimide (PI) powder with a primary diameter of 4 μm (P84NT, Evonik Fibers GmbH) was uniformly dispersed in the continuous phase prior to any oil addition.

To create a HIPPE, the dispersed phase concentration must exceed the maximum packing fraction of the droplets. In this study, oil concentrations (dispersed phase) of 75 and 80 vol % were employed. While not reported here for the sake of conciseness, the torque evolution during emulsification clearly demonstrated the achievement of a concentrated emulsion state when a sharp increase in torque was indeed recorded and showed ratios of final/initial torques of 3 to 10. The continuous phase comprised aqueous solutions of PVA at 2, 3, and 4 wt % and adequate amounts of PI to cover the oil droplets. Based on the expected droplet size range, three levels of PI concentrations were determined to ensure full drop coverage. All emulsions were prepared based on the full factorial design of all variants summarized in Table 1.

Table 1. Variants and Level for Formulation

	level 1	level 2	level 3
PVA solution (wt %)	2	3	4
PI (g)	0.7	0.8	0.9
oil (vol %)	75	80	(−)

The PI volume fraction, which is employed for all results, is calculated based on its volume in the continuous phase. The density of PI is 1.4 g/cm^3, and the volume of the continuous phase is 2 and 2.5 mL for emulsions prepared with 80 and 75 vol %, respectively. Resulted in 6 PI vol % in two different continuous phase volumes (20−23−25 vol % for 75 vol %, and 25−28−32 for 80 vol % oil fraction samples).

2.2. Emulsification. *2.2.1. Emulsification Setup and Procedure.* The high internal phase Pickering emulsions were prepared by using a 3D-printed double-helical ribbon within a 20 mL tank. The required quantity of particles was initially dispersed in the PVA solution by subjecting the mixture to 100−150 rpm for 1 min. Subsequently, the oil was injected at a constant flow rate of 2.5 mL/min, while agitation was maintained. The oil injection port was located at the base of the side wall of the tank (see Figure 1). This configuration allowed the oil to be injected at the bottom of the tank, in the most favorable zone for emulsification at a low impeller speed. The torque meter recorded the data during the mixing process for future calculations. The dimensions of the apparatus are given in Figure 1. These dimensions are representative of efficient ribbon designs, as recommended in the literature.[39]

2.2.2. Processing Conditions. To examine the impact of the emulsification time on the droplet size, three pre-established numbers of revolutions (nr) of the impeller were applied consistently during the emulsification process. The number of revolutions corresponds to the rotational speed multiplied by the emulsification time. This approach is justified by the fact that the HIPPE emulsification process operates in the laminar regime due to the very high viscosity of the concentrated emulsion. In this viscous flow regime, it is the amount of shear
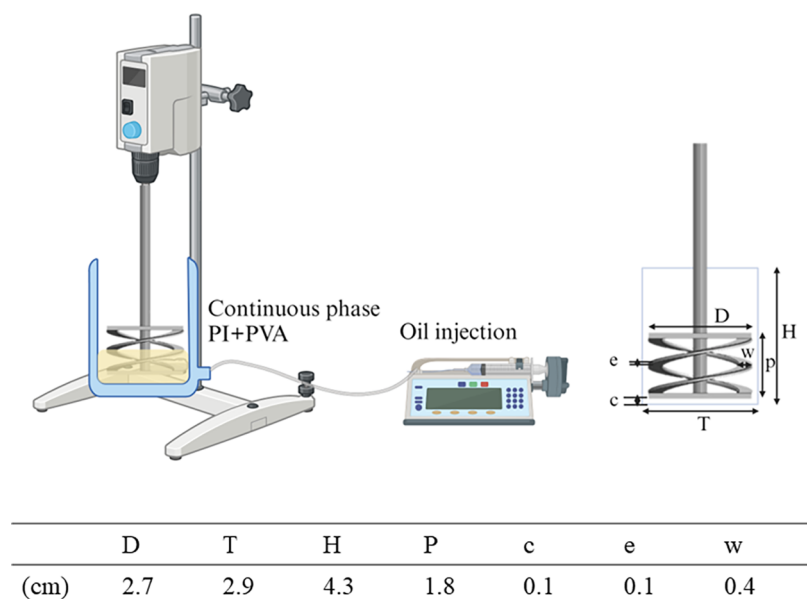
	D	T	H	P	c	e	w
(cm)	2.7	2.9	4.3	1.8	0.1	0.1	0.4

Figure 1. Schematics and dimensions of the setup.

stress exerted on the emulsion that is expected to dictate the drop size reduction process. Exploiting the very high viscosity and the laminar regime, we can relate the number of rotations of the impeller to the potential of droplet rupture. The maximum torque value measured at the end of the emulsification step allows us to access average stress which in turn is related to the energy consumption.

Two values of rotational speeds, chosen for their ability to supply ample pumping capacity within the tank, were employed. The first selected revolution number is much larger than the dimensionless mixing time reported for helical ribbons in the literature.[40] Six process conditions (C1−C6) corresponding to each formulation and three replication runs were conducted for each experiment. The list is presented in Table 2.

Table 2. Process Conditions

condition number	rotational speed (N (rpm))	number of revolutions (nr)	emulsification time (min)
C1(100/800)	100	800	8
C2 (100/1600)		1600	16
C3 (100/2400)		2400	24
C4(150/800)	150	800	5.33
C5 (150/1600)		1600	10.66
C6 (150/2400)		2400	16

The emulsions being viscous with non-Newtonian behavior, the shear rate is defined as per the Metzner and Otto concept following

$$\dot{\gamma} = K_s N \tag{2}$$

where $\dot{\gamma}$ is the shear rate, N is the impeller rotation per second, and K_s is the Metzner and Otto constant. K_s represents the capacity of a given impeller geometry to generate shear at a given rotational speed. Despite being called a "constant", this impeller characteristic may sometimes vary with the flow

behavior index of the fluid (n) in the power-law expression of the viscosity.[28] Based on the published values[41,42] from the literature and the double-helical ribbon geometry used here, we assumed an average K_s value of 30 from the Brito-De La Fuente et al.[42] for a similar geometry and considering the flow behavior index (n) between 0.6 and 0.8.

2.3. Methodology. This section introduces the equations used for estimating the viscosity of the continuous phase for two different approaches: formulation and in situ torque measurement. For formulation-based viscosity estimations, measurements of the PI particle size distribution (PI PSD), the ζ-potential at different PVA concentrations, and the PVA viscosity are required. For torque-based viscosity, the emulsion's torque is recorded during mixing and is correlated to the continuous phase viscosity through analytical equations.

2.3.1. Emulsion Characterization. 2.3.1.1. Determining Droplet Size and Particle Size. Particle and droplet sizes were assessed using dynamic laser diffraction (DLS) with the Mastersizer 3000 instrument from Malvern Panalytical, U.K. The Malvern software provided various droplet size parameters, including D_{10}, D_{50}, and D_{90}, which represent sizes at which 10, 50, and 90% of the volume of all droplets are smaller, respectively. Additionally, the mass-weighted average size (D_{43}) was reported, which best represents the total droplet size within the emulsion. It is given by

$$D_{43} = \frac{\sum_{i=n}^{i=m} n_i D_i^4}{\sum_{i=n}^{i=m} n_i D_i^3} \tag{3}$$

2.3.1.2. Determining Fractal Dimension of Particles. To identify the particle aggregation structure after emulsification, a 2 mL sample of the produced emulsion was collected from the mixing tank and diluted with water. The dilution was performed in a 20 mL tank with the DHR rotating at 100 or 150 rpm for 1 min. Free particles were collected at the bottom of the tank once the agitation was stopped and the mixture had settled. The fluid used to transport the samples during analysis had the exact same composition as the continuous phase (PVA solution at different percentages) to minimize agglomeration or dispersion due to ionic strength changes.

Table 3. Properties of the Continuous Phase

PVA wt %	ζ-potential (mV)	conductivity (mS/cm)	permittivity ($\times 10 \times 10^{-10}$)[a]	particle radius[b] (μm)	viscosity of PVA solution (mPa·s)[c]	$[\eta]$
2	26.68 ± 2.85	0.309	6.9	2.53 ± 0.18	7.3 ± 0.8	2.500
3	55.47 ± 5.8	0.39	6.8	1.31 ± 0.07	23.1 ± 1	2.501
4	132.98 ± 14.9	0.53	6.8	0.83 ± 0.13	61.2 ± 3	2.503

[a]Obtained from ref 46. [b]Particle size for suspension of PI at different PVA solutions. [c]Measured by rheometer; viscosity is constant at 0.1−100 s⁻¹.

The slope of the log−log intensity-scattering angle (I vs q) graph obtained from the DLS corresponds to the fractal dimension, D_f, in eq 4[43,44]

$$I(q) \propto q^{-D_f} \tag{4}$$

The slope is estimated in the domain where $R_g \times q > 5$ where the relation is linear.[43] R_g is the particle gyration radius (half of D_{43}), q is the scattering angle, and I is the scattering intensity.

The compactness of aggregation is represented by the structure prefactor, k_g (eq 5)

$$n_p = k_g \left(\frac{R_g}{r_0} \right)^{D_f} \tag{5}$$

where n_p is the aggregate's particle number and r_0 is the primary particle's radius, which was set at 0.33 μm based on minimum D_{10}, which was observed for the PI particle at PVA 4 wt %. The cubic ratio of R_g/r_0 is used to estimate n_p, since a fully spherical aggregate with a gyration radius R_g contains n_p individual spheres of radius r_0.

2.3.1.3. Scanning Electron Microscopy. Two scanning electron microscopes were used to study and characterize the morphology of the polyimide particles: a Tabletop SEM Hitachi at 5−15 kV, for statistical analysis, as well as an ultrahigh-resolution SEM Hitachi (Regulus 8220) at 2 kV for a more accurate description of the texture at higher resolution. Polyimide particles were analyzed before any process and after the emulsification process. A 2 mL sample of the produced emulsion was collected from the mixing tank and diluted with water. The dilution was performed in a 20 mL tank with the DHR rotating at 100 or 150 rpm for 1 min. The samples were then frozen at −80 °C for 1 h and subjected to freeze-drying for 5 days.

2.3.1.4. ζ-potential of Particle Dispersion in PVA Solutions. The particle's ζ-potential is obtained using a Zetasizer (Malvern Panalytical, U.K.). First, the natural pH of the PVA solutions (2, 3, and 4 wt %) was measured at 6.08, 5.88, and 5.7, respectively. At a concentration of 5 mg/mL and a temperature of 25 °C, at least three distinct samples of each suspension were measured. Folded capillary cells DTS1070 were utilized. The equipment determined the electrophoretic mobility, and the software subsequently applied the Smoluchowski model to calculate the ζ-potential.

2.3.1.5. Surface and Interfacial Tension. To measure surface and interfacial tension between two liquids, the Wilhelmy plate method was employed (DCAT 25, Data Physics Instruments).

2.3.1.6. PVA Viscosity. The viscosity of the PVA solution was measured using a rheometer (MCR 501, Anton Paar) with a double-gap geometry (DG). The viscosity was determined by means of a shear sweep ranging from 0.1 to 100 s⁻¹.

2.3.2. Estimating the Viscosity of the Continuous Phase.
2.3.2.1. Formulation-Based Approach. To estimate the viscosity of the continuous phase based on the formulation,

the intrinsic viscosity of the particle suspension in the continuous phase is determined by the Smoluchowski, Krasny-Ergen equation for large double-layer colloidal suspensions[45]

$$[\eta] = 2.5 \left(1 + \frac{3\varepsilon^2 \zeta^2}{K \mu_c R_g^2} \right) \tag{6}$$

where ε is the absolute permittivity in electromagnetism, ζ is the zeta potential of the particles, K is the specific conductivity of the continuous phase, R_g is the particle radius, and μ_c is the viscosity of the continuous phase alone.

The calculated intrinsic viscosity $[\eta]$, based on (eq 6), is summarized in Table 3.

The concentrated suspension viscosity is determined using the equation used by Pal[47]

$$\eta_r = [1 - k\varphi]^{-[\eta]} \tag{7}$$

where η_r is the relative viscosity. The value of k is obtained as follows

$$k = 1 + \left(\frac{1 - \varphi_m}{\varphi_m^2} \right) \varphi \tag{8}$$

Here, φ_m is the maximum sphere packing factor. Assuming random closed packing for polyimide particles after obtaining the PSD, φ_m is estimated at 0.637.[47] By substitution of eqs 6 and 8 into 7, the relative viscosity of the continuous phase was estimated. The result from eq 7 multiplied by the measured PVA viscosity allows calculation of the complete continuous phase viscosity. This calculation was performed at the three PVA concentrations used in this work.

2.3.2.2. Torque Measurement Approach. To estimate the viscosity of the continuous phase, we first measure the emulsion viscosity. During the mixing procedure, the torque's evolution over time is recorded. There is a correlation between the amount of torque and the viscosity of the samples. In the laminar flow regime, for any specific impeller geometry, the product of Reynolds number (Re) and the power number Np is a constant and is expressed as[39]

$$K_p = Np \times Re = \frac{2\pi N \Gamma}{\eta_e \times N^2 D^3} \tag{9}$$

where η_e is the emulsion viscosity at a specific rotational speed (N), D is the impeller diameter, and Γ is the torque obtained from the torque meter. The useful value of Γ is measured when the torque reaches a plateau at the end of the emulsification process. This maximum value is employed to calculate η_e. In the laminar regime, the K_p value is simply the proportionality constant between Re and Np and represents the capacity of the impeller's geometry to consume power during rotation.

The relative viscosity of the emulsion was estimated by employing again the Pal equation.[47] In this situation, the value of φ_m is the maximum closed-packed droplet volume fraction.
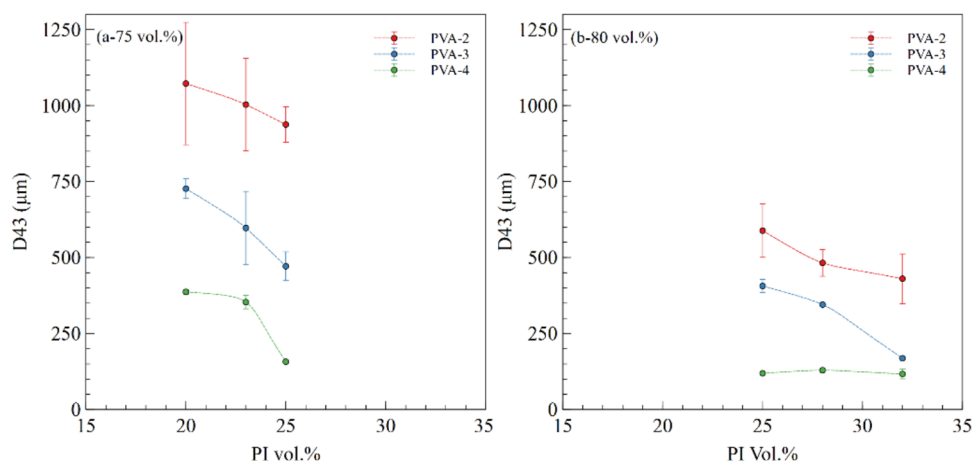
Figure 2. D_{43} for samples prepared under conditions C1(100/800) for 2, 3, and 4 wt % PVA; (a) 75% oil, (b) 80% oil. The results showed that they are based on the volume fraction of PI in the continuous phase at predetermined levels (from Table 1).
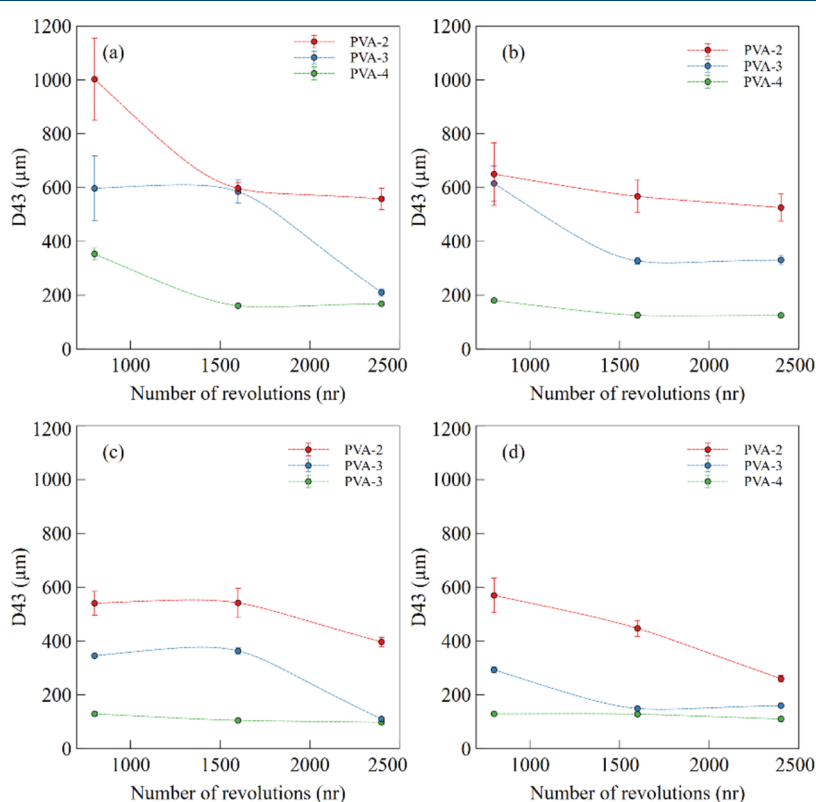

Figure 3. Evolution of D_{43} with respect to the number of revolutions while varying oil fraction, PI, and impeller speed; (a) 75% oil, 23% PI, 100 rpm; (b) 75% oil, 23% PI, 150 rpm; (c) 80% oil, 28% PI, 100 rpm; (d) 80% oil, 28% PI, 150 rpm.

Depending on the emulsion uniformity,[47] it is between 0.68 and 0.86. For closed-packed monodispersed spherical droplets, the φ_m value should be 0.74.[48] In our case, owing to the polydispersity of the prepared HIPPEs, the φ_m value of 0.86 is selected (detailed information is given in Supporting Information Section S1).

$$\eta_r\left[\frac{2\eta_r + 5p}{2 + 5p}\right]^{3/2} = \left[1 - \left(1 + \left(\frac{1 - \varphi_m}{\varphi_m^2}\right)\varphi\right)\varphi\right]^{-2.5} \quad (10)$$

By substituting $\eta_r = \frac{\mu_e}{\mu_c}$ and $p = \frac{\mu_d}{\mu_c}$, where η_e is obtained from eq 8 and η_d is 0.0966 (Pa·s), the viscosity of the continuous phase viscosity is estimated.

3. RESULTS

3.1. Effect of Particle Volume Fraction and Viscosity Modifier (PVA) on Droplet Size. Under comparable processing conditions, the droplet size is generally more impacted by the PVA concentration than the PI concentration. Figure 2 illustrates this general trend where droplet size is more impacted by the PVA concentration versus the PI vol % at the C1(100/800) condition.

With 75% dispersed phase (Figure 2a) and 20 vol % of PI, D_{43} decreased from 1100 to 400 μm by increasing the PVA content from 2 to 4 wt %, respectively. The increase in the oil volume from 75% to 80% (Figure 2b) leads to a sharp decrease in droplet size. For instance, at a constant PI of 25 vol % and for PVA concentration of 2 wt %, the droplet size decreases from 900 to 600 μm with this change in oil from 75 to 80%. However, for emulsions prepared using PVA 4 wt %, increasing the oil vol % did not result in such a sharp reduction in droplet size when 80% was used. It reveals that the droplet reaches its minimum size even at 75 oil vol % with 25 vol % of PI. Beyond this volume fraction, there is no further reduction in droplet size with increasing particle content. It means the system has reached its maximum size reduction capacity. During our preliminary experiments, we ran emulsification tests with 28% PI and 75% oil. The D_{43} obtained then was comparable to the D_{43} obtained at 25% and supports our statement that the minimum size is achieved at 25% PI when using PVA 4%. This observation made us confident that the minimum size of the drops was obtained at the conditions we are using. Moreover, the droplet size does remain constant at PVA 4% and higher oil concentration.

3.2. Effect of Process Condition and Viscosity Modifier (PVA) on Droplet Size.

Figure 3 illustrates the effect of the revolution number at three PVA percentages on the droplet size. It reveals that at constant PI vol %, increasing nr reduces the droplet size down to a minimum; however, the decline in D_{43} depends on PVA wt %, oil volume, and rotational speed. For instance, in Figure 3a, D_{43} is almost constant between 1600 and 2400 revolutions for PVA concentrations of 2 and 4 wt %, whereas at this revolution number for emulsion with PVA 3, droplet size decreases sharply from 600 to 250 μm.

It is also observed that the final value of D_{43} at an nr of 2400 is a function of the viscosity ratio. PVA4, which has the highest continuous phase viscosity, shows the minimum D_{43} for all rotational speeds and oil volume content. Higher oil volume content leads to a minimum D_{43} even at the beginning of the process at 800 revolutions. These findings indicate that impeller speed is less important than the formulation since continuous phase viscosity determines the minimum droplet size. We mentioned earlier that deformation is the leading breakup mechanism in the viscous flow regime, and the results shown here are going along that line.

3.3. Effect of Formulation on the Viscosity of the Continuous Phase.

In Section 2.3, Table 3, we demonstrated that adding PVA changes the continuous phase conductivity and alters the particle radius and ζ-potential. The intrinsic viscosity of the continuous phase is calculated based on eq 6 and summarized in Table 3.

Figure 4 presents the effect of PI vol % on the continuous phase viscosity, which is calculated based on eqs 7 and 8. In general, a higher particle volume fraction increases the viscosity of the continuous phase, which is also amplified with higher PVA content. The presence of PVA exerts a more pronounced impact than does the PI volume fraction. Specifically, for the same PI volume fraction, the viscosity of the continuous phase at PVA 4 wt % is 10-fold higher than that at PVA 2 wt %.

3.4. Effect of Process Conditions on the Viscosity of the Continuous Phase.

The effective viscosity of the continuous phase is obtained through the steps described in Section 2.3.2. The evolution of the effective viscosity of the continuous phase (μ_c) is plotted as a function of the number of
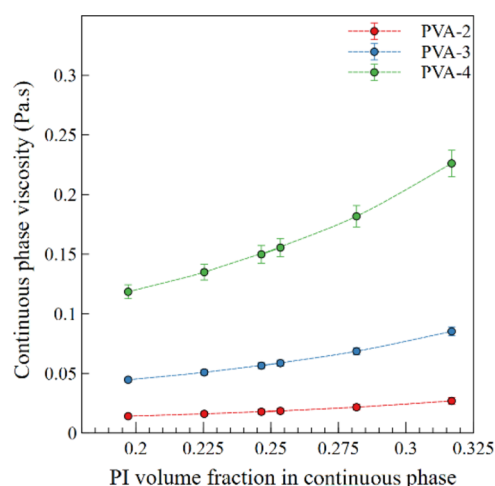

Figure 4. Effect of the PI volume fraction and PVA content on the viscosity of the continuous phase.

revolutions (Figure 5). The results are categorized into four groups with two values of oil volumes and rotational speed. Each point represents the average of the continuous phase viscosity for different PI concentrations under constant conditions. The results show that the variation of viscosity with nr is not constant at each PVA concentration. The viscosity of PVA 2 wt % is almost constant, whereas PVA 3 and 4 generally exhibit radical changes with a changing number of revolutions.

The increased viscosity observed for PVA 4 in Figure 5c for 2400 rpm can be attributed to the generation of very fine droplets and the formation of a strong network of continuous phases around these droplets. Conversely, the decrease observed in Figure 5d for 2400 revolutions might be linked to particle contamination resulting from prolonged exposure to high shear. Contaminated particles are unable to stabilize oil droplets effectively, leading to excess oil observed in the emulsification process and consequently reducing the viscosity.

3.5. Size Evolution of the Remaining Particles in the Continuous Phase.

The particle size distribution (PSD) of the remaining (unattached) PI particles was measured after emulsification. We observed that certain groups of operating conditions generated comparable PI PSD, with peaks at a similar particle size. Figure 6 presents the PSD of these remaining particles according to three distinct groups of conditions that we were able to differentiate. Generally, the three groups offer PSDs with two clear peaks. The first peak (P1, smaller sizes) is the same under all conditions and for all experiments. It corresponds to the individual particle size provided by the supplier. The second peak shifts to smaller particle sizes with extended processing durations (higher nr), higher shear rates (higher rpm), or higher oil and PVA concentrations. This size reduction of the larger particles indicates that the processing conditions break down larger aggregates to generate finer particles.

To illustrate our observation, we use what we determined as Group 1 (G1). For that group, similar particle size distributions with the second peak at 4.2 μm were obtained for unattached particles from emulsions prepared under C1(100)/800 conditions at three different PVA percentages. The combination of low to moderate PVA concentration and prolonged processing time (C3 and C6) shifts the PI PSD to a smaller particle size, and the second peak occurred at 4.0 μm.
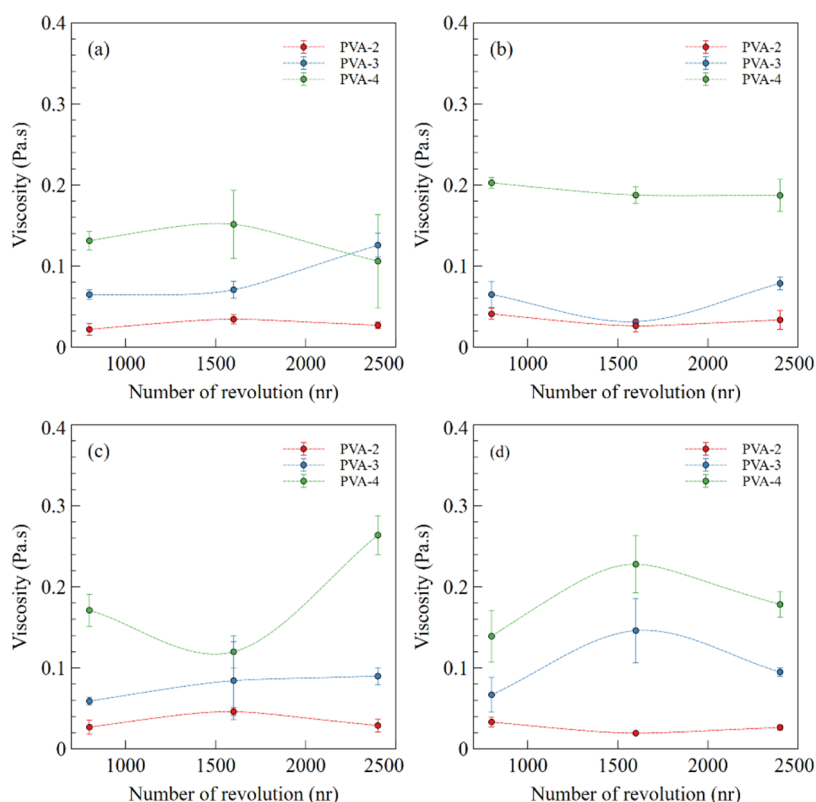
Figure 5. Viscosity of continuous phase as a function of nr; (a) 75% oil, 23% PI, 100 rpm; (b) 75% oil, 23% PI, 150 rpm; (c) 80% oil, 28% PI, 100 rpm; (d) 80% oil, 28% PI, 150 rpm. Note: The lines joining the data points in the graphs serve as a visual guide and do not represent any specific trend.
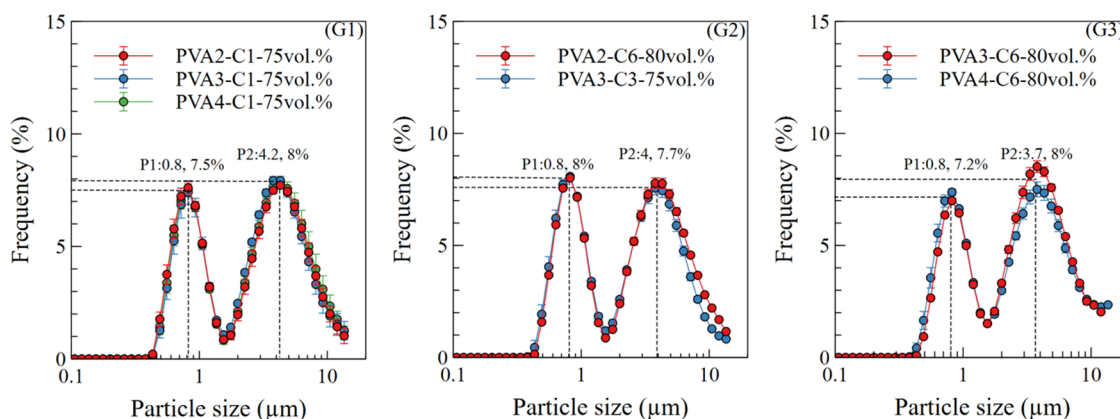

Figure 6. Size distribution of PI particles in three defined groups G1 (low to high viscous (PVA 2, 3, 4 wt %) low-intensity process (100 rpm or 800 nr)); G2 (medium viscous (PVA 2, 3 wt %) medium intensity process (150 rpm for PVA 2 wt %, 100 rpm PVA 3)); G3 (high viscous (PVA 3,4 wt %, 80 oil vol %) high-intensity process (2400 nr and 150 rpm)).

The emulsions prepared with this particle size are placed in Group 2 (G2). Finally, a high-intensity process (higher rpm and nr) or higher viscosity (higher PVA and oil) yields finer particles with P2 at 3.7 μm; these emulsions are categorized in Group 3 (G3). Further emulsions, which were prepared under similar conditions, also showed the same results. The details of formulations and processes are summarized in Supporting Information Table S2.

The shift of PI PSD from G1 to G3 decreases D_{43} of particle, which is considered as a double gyration radius of the particle. From the Mastersizer data, the average of D_{43} for G1 to G3 is 3.69 ± 0.03, 3.41 ± 0.01, and 3.37 ± 0.03, respectively.

The reduction of particle size with higher PVA content is attributed to its role as an electrolyte in the continuous phase, increasing the ζ-potential of particle dispersion and inducing a repulsive interaction that diminishes particle aggregation sizes.[49]

To further characterize the PI aggregates and quantify their compactness, we also measured the fractal dimension (D_f) and structure prefactor (K_g) using the correlation between the intensity and the scattering angle (eq 4). Based on the processing conditions and formulation, the same three groups as the ones based on PSD were investigated. Figure 7 shows the intensity versus scattering angle for the determined groups. The intensity is a linear function of the scattering angle, with
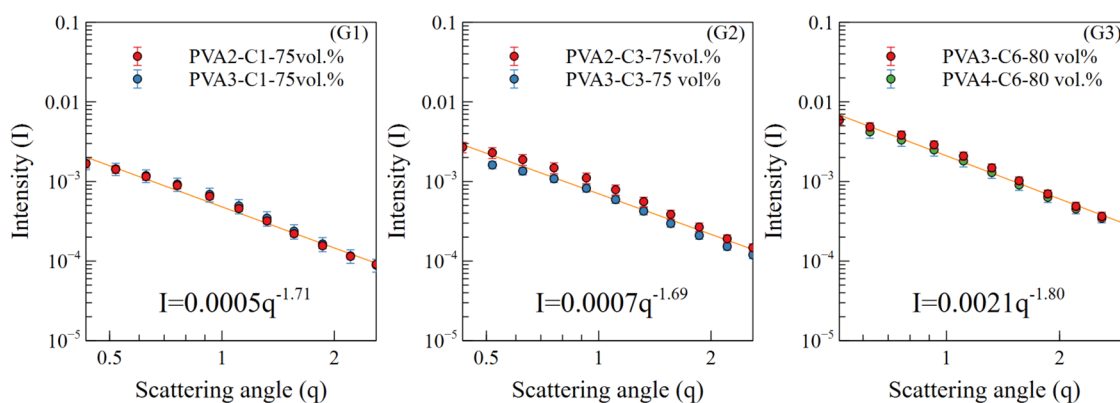
Figure 7. Intensity (I) versus scattering angle (q) for samples in the three groups.

Table 4. Grouping of Particles Following Their Characterization Based on Equation 5

	conditions[a] rpm/nr/oil vol %/PVA wt %	D_f	R_g (μm)	np	k_g
G1	100−150/800−1600/75/2	1.71	1.85 ± 0.015	175 ± 4	9.21 ± 0.25
G2	100/2400/75−80/3	1.69	1.70 ± 0.005	138 ± 1	8.6 ± 0.08
G3	150/1600−2400/80/4	1.80	1.67 ± 0.015	129 ± 3	6.99 ± 0.22

[a]The details of conditions are summarized in the Supporting Information in Table S2.
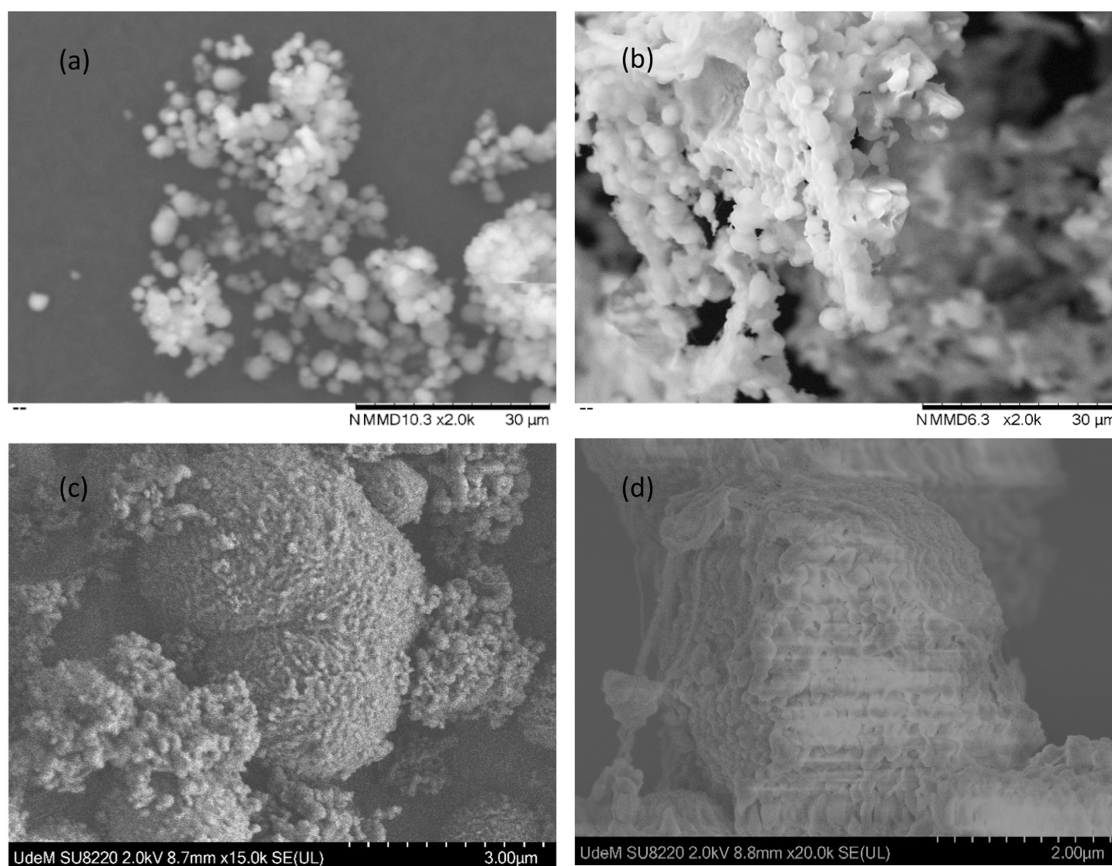

Figure 8. SEM image of (a) pure PI particles and (b) PVA−PI particles; ultrahigh-resolution SEM of (c) pure particles and (d) PVA−PI particles.

D_f corresponding to the exponents on q. It can be noted that group G2 exhibits the lowest D_f value, while group G3 has the highest. A lower D_f value indicates an important presence of nonspherical aggregates in the emulsification process. Under shear, the aggregates can orient or aggregate further depending on the emulsion formulation and process conditions. The aggregation explains the high sensitivity of continuous phase

viscosity and the large variation of the droplet size under shear. Table 4 shows a decrease in the structure prefactor value from G1 to G3, suggesting the reduced compactness of aggregates in G3. A lower compactness enables PVA solutions to penetrate, forming a network with aggregates. This strengthens the continuous phase, facilitating the breakdown and stabilization of finer droplets. It is worth noting that the values of D_f and k_g

are aligned with those found in references dealing with microspherical latex.[50]

3.5.1. Scanning Electron Microscopy (SEM) of Particles. To visualize the effect of process conditions on the particle size and fractal dimensions, SEM images of freeze-dried diluted particles were obtained. Although water evaporation during freeze-drying affects the interaction between PVA and PI particles, comparing the three different processes provides a clear understanding of the particles' shape and size. For consistency, the details of statistical analysis and additional images are provided in the Supporting Information (Section S6); a few images illustrating the effect of PVA on the particles' morphology are shown in Figure 8.

A comparison of Figure 8a,b illustrates that PVA forms a network that surrounds each particle. The surface morphology of both pure and PVA-modified particles, as depicted in Figure 8c,d, confirmed that each PI particle comprises hundreds of nanometer-size particles. This structure allows PVA chains to penetrate due to its porosity.

Table 5 shows that the particle size decreased by higher PVA %, prolonged emulsification process, and higher rotational

Table 5. Statistical Analysis of Microscopic Image

process conditions	size (μm)	aspect ratio
G1	3.34 ± 0.81	1.26 ± 0.16
G2	2.68 ± 0.86	1.15 ± 0.11
G3	2.29 ± 0.45	1.10 ± 0.1

speed; from G1 to G3. The aspect ratio of particles, which is correlated to the fractal dimension, is also decreased by these conditions. These findings confirmed our results obtained from the Mastersizer, showing that particle size reduced through these process conditions from G1 to G3.

3.6. Correlation of Capillary Number with Viscosity Ratio. Figure 9 compares the fitting curve of Ca versus the viscosity ratio p. Figure 9a is obtained based on the formulation approach, and the torque approach is in Figure 9b. In Figure 9a, all samples with constant PVA-oil formulation exhibit constant p value, as the viscosity was solely calculated based on formulation. The calculation of Ca is also based on this viscosity. The low regression coefficient ($R^2 = 0.38$)

observed in Figure 9a indicates the limitation of this approach to accurately estimate Ca. It is worth mentioning that for Figure 9a,b, the interfacial tension decreases slightly with increasing PVA concentration. The interfacial tension between silicon oil (100 cSt) and the three PVA solutions is provided in Supporting Information Table S1.

The viscosity of the continuous phase, estimated solely from the formulation (Section 3.3), leads to a poor correlation between p and Ca. The data in Figure 9a fits on $Ca = -0.005 \log(p) + 0.0165$ with R^2 equal to 0.38, while in Figure 9b, by categorizing data, the correlation matches measurements with R^2 equal to 0.93 and 0.8 were obtained for G1 and G3, respectively. From G1 to G3, the logarithmic slope increased from −0.01 to −0.006, and their intercept decreased from 0.032 in G1 to 0.02, and 0.013 in G2 and G3, respectively. The approach used here clearly helps to represent the behavior of the concentrated emulsions and allows for a fine representation of the droplet size obtained under the concentrated conditions.

To gather all conditions together, we use the same three groups as those presented in 3.5. The process conditions and formulation were summarized in Table S2 in the Supporting Information. In Figure 9b, both nr or rpm and PVA or oil concentration increase from G1 to G3. These conditions lead to smaller PI particles consequently increasing the emulsion's capacity to stabilize droplets. Due to smaller individual particles/agglomerates with the same overall PI vol %, more particles are available for stabilizing finer droplets, which results in a shift of the $Ca-p$ curve toward lower values.

3.7. Estimation of the Droplet Size Based on the Capillary Number and Viscosity Ratio. The droplet diameter (d) was estimated using the following equation by substituting the fitting curve parameters obtained from Sections 3.5 and 3.6 and their corresponding viscosity ratio (p)

$$Ca = a \log(p) + b = \frac{\eta \dot{\gamma}}{2\sigma/D_{43}} \tag{11}$$

Figure 10 compares the estimated and measured droplet sizes. In Figure 10a, values are estimated solely from the formulation, while in Figure 10b, values are determined using the process viscosity obtained from the torque measurements.
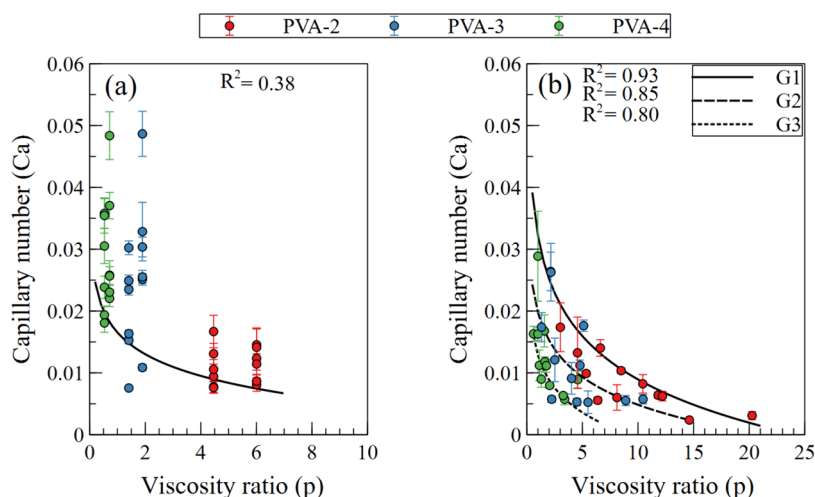

Figure 9. Capillary number vs viscosity ratio (p): (a) calculated based on formulation approach viscosity; (b) calculated based on torque approach viscosity.
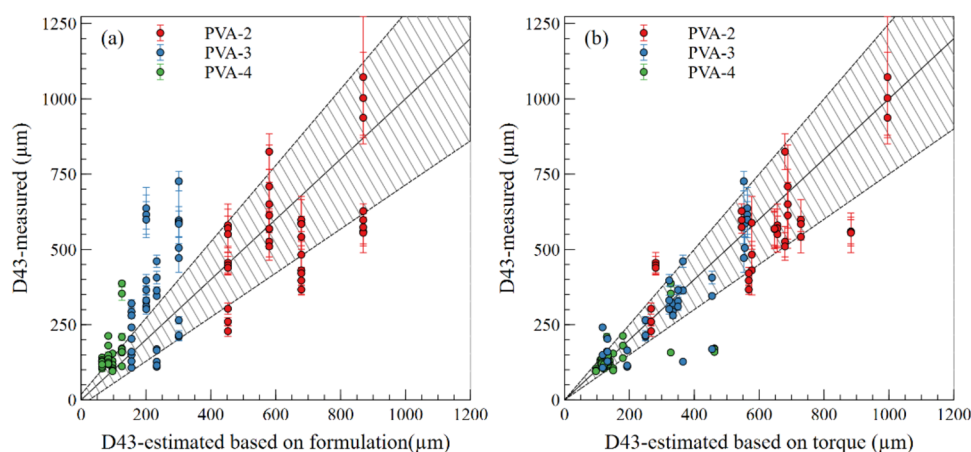
Figure 10. Measured droplet size vs estimated droplet size; (a) estimates based on formulation, (b) estimates based on torque measurement. The hatched area represents the ±25% variation from the line of perfect experimental to estimated match.

The variability is clearly reduced when predicting the droplet size using the process viscosity (torque) compared to the size predicted using the formulation approach. This observation reveals that variations in factors such as the number of revolutions, rotation speed, PVA wt %, and oil concentration affect the ratio of viscous force to interfacial tension (Ca). Therefore, to accurately determine the Ca number and droplet size, it is imperative to incorporate the real viscosity of the continuous phase.

4. DISCUSSION

We demonstrate that HIPPE can be generated with a controlled droplet size selected *a priori*. We take advantage of the highly viscous systems provided by high concentrations of the dispersed phase to reduce the droplet size instead of using high-intensity mixers. The results also reveal that the PVA concentration, the number of revolutions (nr), shear rate, and oil volume all altered the viscosity of the continuous phase. Our results indicate that assuming a constant viscosity of the continuous phase under different process conditions might lead to prediction errors. It is rather crucial to consider the continuous phase viscosity variations in high internal phase emulsions.

Based on the literature, the critical capillary number is a function of the viscosity ratio (p) and the type of flow. In a simple shear flow, Ca decreases with p until it reaches a minimum value (0.5−1) at 0.1 < p < 1. After this minimum, it increases sharply. It is generally agreed that droplet breakage is impossible at p > 3.5 within a simple shear flow.[51] Conversely, in elongational flow, Ca decreases with p and it reaches its minimum (0.1−0.5) at p > 10.[52,53] In such a flow, droplet breakage is considered feasible at all p ranges.

There is a lack of knowledge for estimating Ca in highly concentrated emulsions, especially emulsions where droplets are covered by particles as is the case in HIPPE. The calculated Ca values decrease from 0.03 to 0.005 when the *p-value* increases from 1 to 20. Drops breakage can therefore originate from a combination of simple shear and elongational flows. This is the very nature of tank mixing, where simple flow fields (shear and/or elongational) do not exist alone but in combination and at various degrees. Considering that emulsification in HIPPEs occurs in the presence of very high (overall) viscosity in the laminar regime, it is reasonable to assume that most of the droplet rupture will originate from

elongation. The fact that the drop size reached small values, even at high-viscosity ratios, is an additional argument in favor of a generally elongational flow field in the tank.

The Ca results obtained for HIPPEs are much smaller than the minimum Ca reported for elongational flow, 10 times smaller than Grace's results.[51] This might be attributed to the high interaction between droplets in the HIPPE emulsions and the stabilization process, which involves particle absorption. The Ca−p curves shift to a lower amount by decreasing the particle size. From G1 to G2, finer particles stabilize smaller droplets, leading to lower Ca at a fixed viscosity ratio.

The structure of the particles under all formulations and process conditions plays a crucial role in determining the capillary number. From G1 to G3 in Figure 9, Ca shifts to a lower value by decreasing the k_g and R_g. It reveals that the lower compactness of aggregates (k_g) enhances the penetration of PVA chains into the aggregates, thereby increasing the droplet stability. Additionally, using finer particles, smaller R_g, provides more coverage potential for stabilizing small droplets. Consequently, this leads to the formation of finer droplets at a lower Ca.

The lowest fractal dimension (D_f) belongs to G2 (Table 4), which means that the aggregated structure is far from a spherical likelihood. It is reported that suspension containing plate-like aggregates exhibits complex non-Newtonian behavior owing to the potential of clustering or orientations.[31] Therefore, the continuous phase containing this type of particle is more sensitive to the shear rate.

On the other hand, the intermediate k_g value in G2 allows PVA chains to penetrate. The penetration of PVA chains leads to the clustering or networking of particles, depending on the process conditions. So, the capillary number of the emulsions stabilized with these particles fits into the G2 curve, which lies between the other curves with the largest and finest particles.

In conclusion, the structure of the particles, which is determined by D_{43}, D_f, and k_g, is the key factor for distinguishing the three curves in the Ca−p graph. The finer and less dense the particles, the finer droplets obtained, resulting in a shift of the Ca−p curve to a smaller value.

5. CONCLUSIONS

The droplet size can be tailored in HIPPEs through formulation and process conditions. It showed that the evolution of particle aggregation structure, which is influenced

by the number of revolutions of the impeller, the shear rate, and varying PVA concentrations, significantly impacts the final droplet size. Furthermore, this study highlights the fact that the capillary number is a function of the effective viscosity of the continuous phase and changes with process conditions, emulsification time, and formulation. As a result, by considering both particle structure and the effective viscosity of the continuous phase, a correlation of Ca vs p was obtained for three groups of emulsions. Using these curves, one can estimate the required continuous phase viscosity and process conditions to achieve the desired droplet size.

The use of the effective viscosity of the continuous phase helps determine accurate estimates of the capillary number (Ca). The effective viscosity of the continuous phase obtained through in situ torque monitoring during the emulsion preparation reveals that both the formulation and the process impact the viscosity of the continuous phase. The torque in situ technique is beneficial for inverse engineering approaches to estimate the correct continuous phase viscosity or shear rate to achieve the desired droplet size.

The fractal dimension (D_f), compactness of particles (k_g), and particle radius (R_g), which are affected by PVA content, process conditions, and emulsification time, play crucial roles in explaining the final droplet size at the conditions explored. The continuous phase's effective viscosity, impacted by particle shape and size, supports the estimation of the capillary-viscosity ratio, leading to a more precise prediction of droplet size.

In summary, this investigation offers a better understanding of the relationship among capillary number-viscosity ratios, particle properties, and processing parameters. The ability to modulate emulsion characteristics through the adjustments of key factors provides valuable insights into the design and optimization of emulsion systems with tailored properties.

ASSOCIATED CONTENT

ⓢ **Supporting Information**

The Supporting Information is available free of charge at https://pubs.acs.org/doi/10.1021/acs.iecr.4c01855.

Polydispersity index and uniformity; particle video microscopy images of samples, Process conditions of samples in all groups defined for plotting Ca vs. p, and SEM images of particles and statistical analysis of them (PDF)

AUTHOR INFORMATION

Corresponding Author

Louis Fradette − Department of Chemical Engineering, Polytechnique Montréal, Montreal, Quebec H3C 3A7, Canada; Email: louis.fradette@polymtl.ca

Authors

Mina Saghaei − Department of Chemical Engineering, Polytechnique Montréal, Montreal, Quebec H3C 3A7, Canada; ⓞ orcid.org/0000-0002-1618-3492

Edith Roland Fotsing − Department of Mechanical Engineering, Polytechnique Montréal, Montreal, Quebec H3C 3A7, Canada

Annie Ross − Department of Mechanical Engineering, Polytechnique Montréal, Montreal, Quebec H3C 3A7, Canada

Complete contact information is available at:

https://pubs.acs.org/10.1021/acs.iecr.4c01855

Notes

NOMENCLATURE

Latin Symbols

a=particle radius dispersed in PVA solutions (μm)
c=close-clearance distance
D=impeller diameter
D_{32}=surface-weighted mean diameter (μm)
D_{43}=volume-weighted mean diameter (μm)
D_f=fractal dimension
e=blade thickness
I=scattering intensity
K=specific conductivity of continuous phase (mS/cm)
K_s=Metzner and Otto constant
k_g=structure prefactor for particle aggregate
N=rotational speed (1/s)
n_p=Number of particles at each aggregate
$P=2\pi N\Gamma$
p=pitch length in the impeller
q=scattering angle
R_g=gyration radius of particle aggregate
r_0=radius of individual particle
T=tank diameter
t=time (s)
w=blade width

Greek Symbols

$\dot{\gamma}$=shear rate (1/s)
μ=viscosity (Pa·s)
σ=interfacial force (mN/m)
ε=absolute permittivity in electromagnetism (F/m)
ζ=ζ-potential (V)
φ=dispersed phase volume fraction (−)
φ_m=maximum packing fraction (−)
Γ=torque (N·m)

Dimensionless Numbers

$nr = N \times t$, number of revolutions

$Ca = \frac{\mu\dot{\gamma}}{2\sigma/d}$, Capillary number

$p = \mu_d/\mu_c$, viscosity ratio

$[\eta] = 2.5\left(1 + \frac{3\varepsilon^2\zeta^2}{K\mu_c a^2}\right)$, intrinsic viscosity

$\eta_r = \frac{\mu_c}{\mu_c}$, and $\eta_r = [1 - k\varphi]^{-[\eta]}$, relative viscosity

$k = 1 + \left(\frac{1-\varphi_m}{\varphi_m^2}\right)\varphi$, constant of volume fraction

$Np = \frac{P}{\rho N^3 D^5}$, power number

$Re = \frac{\rho N D^2}{\mu_c}$, Reynolds number

$K_p = Np \times Re = \frac{2\pi\Gamma}{\mu_c \times N^2 D^3}$, power constant

■ REFERENCES

(1) Pickering, S. U. CXCVI.—Emulsions. *J. Chem. Soc., Trans.* **1907**, *91* (0), 2001−2021.

(2) Gonzalez Ortiz, D.; Pochat-Bohatier, C.; Cambedouzou, J.; Bechelany, M.; Miele, P. Current Trends in Pickering Emulsions: Particle Morphology and Applications. *Engineering* **2020**, *6* (4), 468−482.

(3) Binks, B. P. Particles as Surfactants—Similarities and Differences. *Curr. Opin. Colloid Interface Sci.* **2002**, *7* (1−2), 21−41.

(4) Binks, B. P.; Lumsdon, S. O. Influence of Particle Wettability on the Type and Stability of Surfactant-Free Emulsions. *Langmuir* **2000**, *16* (23), 8622−8631.

(5) Tsabet, È.; Fradette, L. Effect of the Properties of Oil, Particles, and Water on the Production of Pickering Emulsions. *Chem. Eng. Res. Des.* **2015**, *97*, 9−17.

(6) Sabri, F.; Berthomier, K.; Wang, C.-S.; Fradette, L.; Tavares, J. R.; Virgilio, N. Tuning Particle−Particle Interactions to Control Pickering Emulsions Constituents Separation. *Green Chem.* **2019**, *21* (5), 1065−1074.

(7) Wan, B.; Fradette, L. Phase Inversion of a Solid-Stabilized Emulsion: Effect of Particle Concentration. *Can. J. Chem. Eng.* **2017**, *95* (10), 1925−1933.

(8) Hu, Y.; Zou, S.; Chen, W.; Tong, Z.; Wang, C. Mineralization and Drug Release of Hydroxyapatite/Poly(l -Lactic Acid) Nanocomposite Scaffolds Prepared by Pickering Emulsion Templating. *Colloids Surf., B* **2014**, *122*, 559−565.

(9) Wu, J.; Xue, W.; Wang, C.; Gu, H.; Zhou, J.; Lin, W. Bioactive Porous Protein Scaffolds Enabled by High Internal Phase Emulsion Templates. *Ind. Eng. Chem. Res.* **2023**, *62* (44), 18463−18472.

(10) Chen, L.; Ao, F.; Ge, X.; Shen, W. Food-Grade Pickering Emulsions: Preparation, Stabilization and Applications. *Molecules* **2020**, *25* (14), No. 3202.

(11) Rodriguez, A. M. B.; Binks, B. P. Catalysis in Pickering Emulsions. *Soft Matter* **2020**, *16* (45), 10221−10243.

(12) Wei, Y.-S.; Niu, Z.-C.; Wang, F.-Q.; Feng, K.; Zong, M.-H.; Wu, H. A Novel Pickering Emulsion System as the Carrier of Tocopheryl Acetate for Its Application in Cosmetics. *Mater. Sci. Eng., C* **2020**, *109*, No. 110503.

(13) Zhu, Y.; Zhang, R.; Zhang, S.; Chu, Y.; Chen, J. Macroporous Polymers with Aligned Microporous Walls from Pickering High Internal Phase Emulsions. *Langmuir* **2016**, *32* (24), 6083−6088.

(14) Hao, G. P.; Li, W. C.; Qian, D.; Wang, G. H.; Zhang, W. P.; Zhang, T.; Wang, A. Q.; Schüth, F.; Bongard, H. J.; Lu, A. H. Structurally Designed Synthesis of Mechanically Stable Poly-(Benzoxazine-Co- Resol)-Based Porous Carbon Monoliths and Their Application as High-Performance CO2 Capture Sorbents. *J. Am. Chem. Soc.* **2011**, *133* (29), 11378−11388.

(15) Saghaei, M.; Ross, A.; Fotsing, E.-R.; Fradette, L. Creating Optimized Acoustic Structure Via Concentrated Emulsions. *Can. Acoust.* **2023**, *51*, 148−149.

(16) Yi, F.; Xu, F.; Gao, Y.; Li, H.; Chen, D. Macrocellular Polymer Foams from Water in Oil High Internal Phase Emulsion Stabilized Solely by Polymer Janus Nanoparticles: Preparation and Their Application as Support for Pd Catalyst. *RSC Adv.* **2015**, *5* (50), 40227−40235.

(17) Yang, T.; Hu, Y.; Wang, C.; Binks, B. P. Fabrication of Hierarchical Macroporous Biocompatible Scaffolds by Combining Pickering High Internal Phase Emulsion Templates with Three-Dimensional Printing. *ACS Appl. Mater. Interfaces* **2017**, *9* (27), 22950−22958.

(18) Zhao, X.; Cui, Y.; Wang, J.; Wang, J. Preparation of Fluorescent Molecularly Imprinted Polymers via Pickering Emulsion Interfaces and the Application for Visual Sensing Analysis of Listeria Monocytogenes. *Polymers* **2019**, *11* (6), No. 984.

(19) Bago Rodriguez, A. M.; Binks, B. P. High Internal Phase Pickering Emulsions. *Curr. Opin. Colloid Interface Sci.* **2022**, *57*, No. 101556.

(20) Albert, C.; Beladjine, M.; Tsapis, N.; Fattal, E.; Agnely, F.; Huang, N. Pickering Emulsions: Preparation Processes, Key Parameters Governing Their Properties and Potential for Pharmaceutical Applications. *J. Controlled Release* **2019**, *309*, 302−332.

(21) Köhler, K.; Santana, A. S.; Braisch, B.; Preis, R.; Schuchmann, H. P. High Pressure Emulsification with Nano-Particles as Stabilizing Agents. *Chem. Eng. Sci.* **2010**, *65* (10), 2957−2964.

(22) Wu, J.; Ma, G.-H. Recent Studies of Pickering Emulsions: Particles Make the Difference. *Small* **2016**, *12* (34), 4633−4648.

(23) Xu, Q. Y.; Nakajima, M.; Binks, B. P. Preparation of Particle-Stabilized Oil-in-Water Emulsions with the Microchannel Emulsification Method. *Colloids Surf., A* **2005**, *262* (1−3), 94−100.

(24) Zalc, J. M.; Szalai, E. S.; Muzzio, F. J.; Jaffer, S. Characterization of Flow and Mixing in an SMX Static Mixer. *AIChE J.* **2002**, *48* (3), 427−436.

(25) Kritikos, A.; Singh, R.; Tsilomelekis, G.; Muzzio, F. J. A Novel CFD Model of SMX Static Mixer Used in Advanced Continuous Manufacturing of Active Pharmaceutical Ingredients (API). *J. Pharm. Innov.* **2024**, *19* (2), No. 14, DOI: 10.1007/s12247-024-09813-1.

(26) Holdich, R. G.; Ipek, I. Y.; Lazrigh, M.; Shama, G. Production and Evaluation of Floating Photocatalytic Composite Particles Formed Using Pickering Emulsions and Membrane Emulsification. *Ind. Eng. Chem. Res.* **2012**, *51* (38), 12509−12516.

(27) Wan, B.; Tsabet, E.; Fradette, L. Impact of Particles on Breakage and Coalescence Processes during the Preparation of Solid-Stabilized Emulsions. *Ind. Eng. Chem. Res.* **2019**, *58* (14), 5631−5639.

(28) Guntzburger, Y.; Fradette, L.; Farhat, M.; Héniche, M.; Tanguy, P. A.; Takenaka, K. Effect of the Geometry on the Performance of the Maxblend Impeller with Viscous Newtonian Fluids. *Asia-Pac. J. Chem. Eng.* **2009**, *4* (5), 528−536.

(29) Gingras, J. P.; Fradette, L.; Tanguy, P.; Jorda, E. Concentrated Bitumen-in-Water Emulsification in Coaxial Mixers. *Ind. Eng. Chem. Res.* **2007**, *46*, 1818−1825.

(30) Delacroix, B.; Fradette, L.; Bertrand, F.; Blais, B. Which Impeller Should Be Chosen for Efficient Solid−Liquid Mixing in the Laminar and Transitional Regime? *AIChE J.* **2021**, *67* (11), No. e17360, DOI: 10.1002/aic.17360.

(31) Larson, R. G. *The Structure and Rheology of Complex Fluids*; Oxford University Press: Newyork, 1999; Vol. 150.

(32) Alvarez, M. M.; Zalc, J. M.; Shinbrot, T.; Arratia, P. E.; Muzzio, F. J. Mechanisms of Mixing and Creation of Structure in Laminar Stirred Tanks. *AIChE J.* **2002**, *48* (10), 2135−2148.

(33) De Bruijn, R. A. Tipstreaming of Drops in Simple Shear Flows. *Chem. Eng. Sci.* **1993**, *48* (2), 277−284.

(34) Muzzio, F. J.; Tjahjadi, M.; Ottino, J. M. Self-Similar Drop-Size Distributions Produced by Breakup in Chaotic Flows. *Phys. Rev. Lett.* **1991**, *67* (1), 54−57.

(35) Sharma, T.; Kumar, G. S.; Sangwai, J. S. Viscoelastic Properties of Oil-in-Water (o/w) Pickering Emulsion Stabilized by Surfactant−Polymer and Nanoparticle−Surfactant−Polymer Systems. *Ind. Eng. Chem. Res.* **2015**, *54* (5), 1576−1584.

(36) Cheng, X.; McCoy, J. H.; Israelachvili, J. N.; Cohen, I. Imaging the Microscopic Structure of Shear Thinning and Thickening Colloidal Suspensions. *Science* **2011**, *333* (6047), 1276−1279.

(37) Lee, C. H.; Moturi, V.; Lee, Y. Thixotropic Property in Pharmaceutical Formulations. *J. Controlled Release* **2009**, *136* (2), 88−98.

(38) Malkin, A. Y.; Masalova, I.; Slatter, P.; Wilson, K. Effect of Droplet Size on the Rheological Properties of Highly-Concentrated w/o Emulsions. *Rheol. Acta* **2004**, *43* (6), 584−591.

(39) Paul, E. L.; Atiemo-Obeng, V. A.; Kresta, S. M. *Handbook of Industrial Mixing*; John Wiley & Sons, Inc: NJ, 2004; Vol. 1.

(40) Delaplace, G.; Leuliet, J. C.; Relandeau, V. Circulation and Mixing Times for Helical Ribbon Impellers. Review and Experiments. *Exp. Fluids* **2000**, *28* (2), 170−182.

(41) Carreau, P. J.; Chhabra, R. P.; Cheng, J. Effect of Rheological Properties on Power Consumption with Helical Ribbon Agitators. *AIChE J.* **1993**, *39* (9), 1421−1430.

(42) Brito-De La Fuente, E.; Choplin, L.; Tanguy, P. A. Mixing with Helical Ribbon Impellers: Effect of Highly Shear Thinning Behaviour and Impeller Geometry. *Chem. Eng. Res. Des.* **1997**, *75* (1), 45−52.

(43) Bushell, G. C.; Yan, Y. D.; Woodfield, D.; Raper, J.; Amal, R. On Techniques for the Measurement of the Mass Fractal Dimension of Aggregates. *Adv. Colloid Interface Sci.* **2002**, *95* (1), 1−50.

(44) Lazzari, S.; Nicoud, L.; Jaquet, B.; Lattuada, M.; Morbidelli, M. Fractal-like Structures in Colloid Science. *Adv. Colloid Interface Sci.* **2016**, *235*, 1−13.

(45) Krasny-Ergen, W. Untersuchungen Über Die Viskosität von Suspensionen Und Lösungen. 2. Zur Theorie Der Elektroviskosität. *Kolloid-Z.* **1936**, *74* (2), 172−178.

(46) Yeow. Improved Dielectric Model for Polyvinyl Alcohol-Water Hydrogel at Microwave Frequencies. *Am. J. Appl. Sci.* **2010**, *7* (2), 270−276.

(47) Pal, R. New Generalized Viscosity Model for Non-Colloidal Suspensions and Emulsions. *Fluids* **2020**, *5* (3), No. 150.

(48) Pal, R. Viscosity−Concentration Equation for Emulsions of Nearly Spherical Droplets. *J. Colloid Interface Sci.* **2000**, *231* (1), 168−175.

(49) Zhou, F.; Zhou, R.; Hao, X.; Wu, X.; Rao, W.; Chen, Y.; Gao, D. Influences of Surfactant (PVA) Concentration and PH on the Preparation of Copper Nanoparticles by Electron Beam Irradiation. *Radiat. Phys. Chem.* **2008**, *77* (2), 169−173.

(50) Johnson, C. P.; Li, X.; Logan, B. E. Settling Velocities of Fractal Aggregates. *Environ. Sci. Technol.* **1996**, *30* (6), 1911−1918.

(51) Grace†, H. P. Dispersion phenomena in high viscosity immiscible fluid systems and application of static mixers as dispersion devices in such systems. *Chem. Eng. Commun.* **1982**, *14* (3−6), 225−277.

(52) Fradette, L.; Tanguy, P.; Li, H.-Z.; Choplin, L. Liquid/Liquid Viscous Dispersions with a SMX Static Mixer. *Chem. Eng. Res. Des.* **2007**, *85* (3), 395−405.

(53) Bentley, B. J.; Leal, L. G. An Experimental Investigation of Drop Deformation and Breakup in Steady, Two-Dimensional Linear Flows. *J. Fluid Mech.* **1986**, *167* (1), 241−283.